Eur. J. Mineral.
2007, **19**, 641–655
Published online October 2007

This paper was presented at the EMPG XI symposium in Bristol, U.K. (September 2006)

An electron microprobe, LAM-ICP-MS and single-crystal X-ray structure refinement study of the effects of pressure, melt-H_2O concentration and fO_2 on experimentally produced basaltic amphiboles

JOHN ADAM[1,*], ROBERTA OBERTI[2], FERNANDO CÁMARA[2] and TREVOR H. GREEN[1]

[1] Department of Earth and Planetary Sciences, Macquarie University, N.S.W., 2109, Australia
*Corresponding author, e-mail: john.adam1@bigpond.com
[2] CNR-Istituto di Geoscienze e Georisorse, unità di Pavia, via Ferrrata 1, I-27100 Pavia, Italy

Abstract: Amphiboles were crystallized in sub-liquidus experiments at 0.5–2.0 GPa and 1000–1050 °C from hydrous nepheline basanite and olivine basalt starting compositions. The amphiboles and coexisting (quenched) melts were analysed for major, minor and trace elements by a combination of electron microprobe, laser ablation microprobe and inductively-coupled plasma mass-spectrometry (LAM ICP-MS). Individual amphiboles were also characterized by single-crystal X-ray structure refinement, and empirical estimates of dehydrogenation were obtained based on M1–M2 distances. The amphiboles display compositional variation that can be interpreted as crystal-chemical responses to: (1) increasing pressure, and (2) changes in oxygen fugacity (fO_2) and the activity of H_2O. As pressure increases, Al moves from the T1 tetrahedron (where it is replaced by Si) to the octahedral M2 site. This coupled substitution, which implies an increase in coordination number for Al, results in a decrease in the *c* and *b* unit-cell edges. The overall decrease in unit-cell volumes is kept small, however, by an increase in the ^{B}(Fe, Mg) content with increasing pressure, which in turn decreases the volume occupied by the B-cations but increases the $\sin\beta$ value. In this way, the entrance of minor K at the A site and Cl at the O3 site (K_Ds for both increase with pressure) is allowed, resulting in a slight lengthening of the *a* edge. The degree of dehydrogenation at O3 correlates inversely with the H_2O concentration in coexisting melts. Generally, dehydrogenation is locally balanced by ^{M1}Ti, with the Ti excess with respect to $^1/_2$ O^{2-} ordered at the M2 site. In one sample, crystallized under more oxidizing conditions, O^{2-} is > 2Ti, and local charge balance requires the presence of Fe^{3+} ordered at the M1 (and M3) sites. $D^{amph/melt}$ values measured for the high field strength elements Ti, Zr, Hf, Nb and Ta (D_{HFSE}) correlate positively with O^{2-} and with $^{[4]}$Al, suggesting that Ti, Zr, Hf, Nb and Ta (HFSE) are incorporated in both the M1 and the M2 sites. Partition coefficients for rare earth elements (D_{REE}) correlate positively with $^{[4]}$Al and negatively with $^{[6]}$Al. Increased fO_2 results in increased Fe^{3+}, $^{[4]}$Al and D_{REE}, but does not produce a noticeable increase in O^{2-} or in D_{HFSE}.

Key-words: experimental petrology, amphibole, basalt, structure refinements, trace elements, water, halogens.

1. Introduction

Under a number of circumstances amphibole is genetically associated with basalts and plays a role in their origin and evolution. Amphibole occurs as phenocrysts and megacrysts in basalts (*e.g.* Irving & Frey, 1984; Rock *et al*., 1991; Wilkinson & Hensel, 1991) and it is also present in some type I peridotite xenoliths (*e.g.* Varne, 1970; Stolz & Davies, 1988; Ionov *et al*., 1997). Thus amphibole can be a fractionating phase from basaltic magmas, and may also be present in their mantle source regions. In these two roles amphibole serves both as a potential repository and source of alkalis, high-field-strength elements (HFSE), H_2O and halogens. In this study, we use a group of amphiboles that were experimentally crystallized from hydrous basaltic melts to examine the interrelationships between amphibole crystal-structure, site occupancies, composition, pressure of synthesis, melt H_2O concentration and fO_2. We also consider how these factors affect the partitioning of trace and minor elements between amphiboles and basaltic melts. The amphiboles were investigated by a combination of X-ray diffraction, electron microprobe, and laser-ablation microprobe and inductively-coupled plasma mass spectrometry (LAM-ICP-MS) techniques. The experimental conditions used to crystallize the amphiboles (Table 1) varied from 0.5 to 2.0 GPa and 1000 to 1050 °C. They also included a range of melt compositions, H_2O starting concentrations (5–12 wt. %) and fO_2 conditions.

2. Experimental and analytical methods

2.1. Starting materials

The three different starting compositions used to grow amphiboles (Table 2) represent a spectrum of mildly to more strongly alkaline basaltic rocks, of broadly sodic character, that are typical of intraplate volcanic settings in many parts of the world (see review of Knutson *et al*., 1989). They include an olivine basalt from Mount Leura in Queensland,

DOI: 10.1127/0935-1221/2007/0019-1750
0935-1221/07/0019-1750 $ 6.75

Table 1. Summary of run conditions and products for the experiments examined in this paper.

Run	starting mix	wt.% H_2O in S. mix			Run product modes (wt. %)								
			GPa	°C	amph	mica	garnet	cpx	opx	ol	mag	ap	gl
1923	ML	10.0	2.0	1050	16	0	8	5	2	0	0	0	67
1941	ML	7.5	1.5	1050	21	0	0	2	5	0	0	0	72
1925	ML	5.0	1.0	1050	12	0	0	7	0	6	0	0	75
1442	SH	10.0	2.0	1050	21	0	0	13	0	0	0	0	66
1541[f]	SH	10.0	2.0	1050	11	0	0	8	0	0	4	0	77
1539	SH	12.0	2.0	1000	40	0	0	0	0	0	0	0	60
1446	SH	10.0	1.5	1050	22	0	0	4	0	0	0	0	74
1447	SH	10.0	1.0	1050	34	0	0	0	0	0	0	0	66
1452	SH	5.0	0.5	1025	36	0	0	0	0	0	0	0	64
1950	BH	10.0	2.0	1050	17	7	0	9	1	0	0	0	66
1951	BH	7.5	1.0	1025	18	0	0	4	0	9	0	0.1	68.9

Run product modes were calculated from mass balances between major element concentrations in run products and starting mixes. Run 1541^f was conducted using a haematite/magnetite fO_2 buffer. Abbreviations for starting mixes are ML = Mount Leura, SH = Southern Highlands, and BH = Bow Hill. Abbreviations for run products are amph = amphibole, cpx = clinopyroxene, ol = olivine, mag = magnetite, ap = apatite, and gl = glass.

Australia, a nepheline basanite from the Southern Highlands of NSW, Australia (Wass, 1980), and a second nepheline basanite from Bow Hill in Tasmania, Australia (Adam, 1990). Amphiboles crystallized from the latter two compositions were produced during earlier experimental studies by Adam & Green (1994, 2006). These include two previously unpublished experiments on the Southern Highlands basanite that are described in this study. Details of the basanite starting material preparations are described by Adam & Green (1994, 2006).

The Mount Leura starting glass was prepared using procedures nearly identical to those described by Adam & Green (2006). Most of the 42 dopants added to the composition were added as aqueous solutions to give a total of 1.52 wt. % of trace oxides in the dry mix. Once thoroughly ground and dried, the mix was melted and quenched to form a glass. Cl, Br and I were added to individual experiments, along with H_2O, in a stock aqueous solution containing 10 000 ppm each of Cl, Br and I (added as potassium halides). Actual Cl concentrations in starting mixes were higher than originally intended. This was a consequence of using Cl-bearing aqueous solutions (ICP MS analytical standards) as a source of dopants. Melting times during preparation of the starting glass were kept brief to avoid the excessive loss of volatile dopants (*e.g.* Mo, Sb and Sn) and consequently Cl was incompletely degassed. Previous experiments by Adam et al. (1993) on a Cl-enriched basanite containing 4.0 wt. % Cl showed no evident effect of this amount of Cl on partition coefficients. Therefore the Cl concentrations in our starting mixes (0.22–0.33 wt. %) were unlikely to have perceptibly affected partition coefficients.

2.2. Experimental apparatus and procedures

The experimental methods used on the Mount Leura olivine basalt were essentially the same as those described by Adam & Green (2006). The experiments were performed in a Boyd & England (1960) type piston-cylinder apparatus using 12.7 mm diameter furnace assemblies and a cold piston-in technique. Furnace sleeves were made of talc and pyrex® with boron nitride inserts. A minus 10 % correction for friction was applied to measured pressures (Green *et al.*, 1966). Temperature was measured using Pt-$Pt_{90}Rh_{10}$ thermocouples and controlled to within a few degrees of the set point by a Leeds & Northrup® Electromax V single-loop controller. All experiments on the Mount Leura olivine basalt were conducted at a temperature of 1050 °C, but to encourage the growth of large crystals run temperatures were originally raised to 1160 °C and maintained at this temperature for 30 min. The temperature was then gradually decreased over a further 30 min to the final run temperature. The total run time for each experiment was 48 h. Experiments were performed at 1.0, 1.5 and 2.0 GPa.

Starting materials were contained in double capsules with an outer Pt capsule and an inner graphite capsule. H_2O and halides were added to individual experiments using a graduated micro syringe. In order to maintain an approximately constant degree of crystallization in all three experiments, the amount of H_2O added was varied from 5 wt. % at 1.0 GPa, to 7.5 wt. % at 1.5 GPa, and 10 wt. % at 2.0 GPa. At the completion of experiments, capsules were removed and sectioned longitudinally. The sections were then mounted in epoxy and polished using non-aqueous solvents. The experimental procedures used for experiments on the Southern Highlands basanite are described by Adam & Green (1994). They were similar to those employed on the Mount Leura and Bow Hill starting compositions, but differed by using unlined $Ag_{70}Pd_{30}$ capsules in place of graphite-lined Pt capsules. Run 1541 on the Southern Highlands basanite was also exceptional because it was conducted in a double $Ag_{70}Pd_{30}$ capsule with a haematite-magnetite fO_2 buffer (see Adam & Green, 1994).

Table 2. Major and minor elements in run products and starting compositions.

GPa	2.0	1.5	1.0	2.0	2.0	2.0	1.5	1.0	2.0
run	1923	1941	1925	1541	1539	1923	1941	1925	1541
	amphiboles					clinopyroxenes			
	Mount Leura			Southern Highlands		Mount Leura			Southern Highlands
n	17	13	15			16	2	10	
SiO_2	42.57 (0.41)	41.30 (0.85)	41.68 (0.29)	41.41 (0.33)	42.59	51.91 (0.73)	49.31 (0.66)	47.55 (1.26)	49.46 (0.49)
TiO_2	2.12 (0.08)	2.75 (0.34)	3.41 (0.11)	1.28 (0.02)	1.83	0.63 (0.16)	0.89 (0.10)	2.21 (0.65)	0.63 (0.15)
Al_2O_3	14.24 (0.40)	13.95 (0.70)	14.17 (0.49)	13.32 (0.12)	13.09	4.22 (1.11)	5.49 (0.21)	7.77 (1.32)	5.73 (0.81)
Cr_2O_3	0.05 (0.03)	0.07 (0.04)	0.09 (0.03)	0.02 (0.02)	0.16	0.09 (0.05)	0.10 (0.02)	0.36 (0.14)	0.11 (0.06)
FeO	8.37 (0.65)	9.32 (0.52)	8.73 (0.18)	8.23 (0.07)	8.55	7.12 (0.65)	7.12 (0.65)	8.75 (0.42)	7.10 (0.37)
NiO	0.03 (0.02)	0.03 (0.03)	0.04 (0.03)	0.27 (0.04)		0.02 (0.02)			0.18 (0.04)
MnO	0.10 (0.02)	0.11 (0.01)	0.12 (0.02)	0.09 (0.02)	0.10	0.16 (0.04)	0.15 (0.01)	0.17 (0.01)	0.12 (0.03)
MgO	15.43 (0.48)	14.72 (0.39)	14.66 (0.31)	16.16 (0.54)	15.09	16.23 (0.74)	15.19 (0.31)	13.38 (0.99)	14.16 (0.69)
CaO	10.29 (0.22)	10.20 (0.36)	10.73 (0.15)	10.94 (0.12)	10.90	18.25 (0.97)	18.14 (0.22)	19.22 (0.53)	21.61 (0.40)
Na_2O*	2.61 (0.10)	2.70 (0.14)	2.64 (0.11)	2.20 (0.12)	2.41	0.86 (0.11)	0.75 (0.04)	0.63 (0.07)	1.01 (0.18)
K_2O	1.29 (0.04)	1.01 (0.09)	0.78 (0.03)	2.07 (0.05)	1.72	0.00 0.00	0.00	0.00	0.00
P_2O_5	0.03 (0.02)	0.05 (0.03)	0.04 (0.02)	0.04 (0.04)		0.00	0.03 (0.00)	0.06 (0.03)	0.03 (0.02)
F	0.19 (0.03)	0.20 (0.01)	0.26 (0.01)						
Cl	0.05 (0.01)	0.07 (0.01)	0.06 (0.00)						
I	0.08 (0.02)	0.08 (0.02)	0.09 (0.00)						
Total	97.45	96.56	97.50	96.03	98.08	99.47	98.89	98.48	99.41
Mg no.	76.7	73.8	75.0	56.1		80.2	75.6	77.1	79.8

GPa	2.0	1.5	1.0	2.0	2.0	2.0	starting glasses		
Run	1923	1941	1925	1923	1923	1541	Mount	Bow	Southern
	orthopyroxenes		olivine	garnet		magnetite	Leura	Hill	Highlands
				core	rim				
n	9	10	5	9	9		11		
SiO_2	52.91 (0.45)	50.48 (0.55)	37.88 (0.28)	39.82 (0.09)	40.20 (0.20)	0.01 (0.00)	48.47 (0.34)	43.88	46.66
TiO_2	0.31 (0.03)	0.44 (0.09)	0.06 (0.02)	1.14 (0.07)	0.65 (0.21)	17.47 (0.02)	2.13 (0.07)	2.32	2.19
Al_2O_3	4.61 (0.79)	5.54 (0.96)	0.03 (0.01)	21.78 (0.14)	22.41 (0.32)	2.05 (0.00)	15.20 (0.21)	11.35	14.09
Cr_2O_3	0.13 (0.04)	0.18 (0.04)	0.02 (0.01)	0.13 (0.06)	0.09 (0.09)	0.23 (0.04)	0.03 (0.02)	0.06	0.07
FeO	12.66 (0.89)	12.43 (1.27)	23.46 (0.63)	14.31 (0.19)	14.50 (0.54)	69.35 (0.13)	10.96 (0.17)	11.71	9.83
NiO	0.06 (0.05)	0.08 (0.04)	0.09 (0.02)			0.10 (0.03)	0.00	0.04	
MnO	0.18 (0.05)	0.18 (0.04)	0.26 (0.02)	0.41 (0.04)	0.41 (0.03)	0.37 (0.01)	0.16 (0.04)	0.19	0.16
MgO	27.26 (0.54)	26.83 (0.66)	37.93 (0.41)	13.92 (0.29)	14.55 (0.47)	3.22 (0.04)	9.15 (0.13)	12.00	8.43
CaO	1.53 (0.27)	2.00 (0.29)	0.17 (0.02)	7.78 (0.21)	6.85 (0.43)	0.01 (0.01)	8.95 (0.13)	9.36	9.62
Na_2O	0.11 (0.03)	0.10 (0.02)	0.01 (0.01)	0.05 (0.02)	0.04 (0.01)	0.00	3.19 (0.07)	4.12	3.50
K_2O	0.00 (0.00)	0.02 (0.01)	0.01 (0.01)	0.00 (0.00)	0.00 (0.00)	0.00	1.15 (0.05)	2.02	2.00
P_2O_5	0.00 (0.00)	0.02 (0.01)	0.04 (0.03)			0.03 (0.00)	0.59 (0.05)	1.43	0.85
Total	99.70	98.41	99.95	99.34	99.70	92.84	99.98	98.60	97.40
Mg no.	79.3	79.1	74.2	63.4	64.1		59.8	64.6	

GPa		2.0	1.5	1.0	2.0	2.0
run		1923	1941	1925	1541	1539
		run product glasses				
		Mount Leura			Southern Highlands	
n		20	13	11		15
SiO_2		44.27 (0.81)	44.44 (0.72)	46.27 (0.19)	35.79 (4.30)	37.98 (1.50)
TiO_2		2.19 (0.08)	1.93 (0.06)	2.01 (0.05)	1.25 (0.22)	1.87 (0.17)
Al_2O_3		14.03 (0.26)	14.66 (0.19)	16.03 (0.08)	12.56 (2.64)	13.14 (1.13)
Cr_2O_3		0.02 (0.02)	0.03 (0.01)	0.02 (0.01)	0.01 (0.01)	
FeO		6.91 (0.45)	9.86 (0.18)	9.26 (0.14)	5.02 (1.06)	7.91 (0.94)
NiO			0.02 (0.01)	0.04 (0.03)	0.13 (0.04)	0.17 (0.06)
MnO		0.10 (0.03)	0.14 (0.02)	0.16 (0.03)	0.05 (0.02)	2.93 (0.52)
MgO		4.93 (0.53)	5.05 (0.08)	4.84 (0.05)	4.65 (1.86)	6.14 (0.74)
CaO		7.07 (0.46)	7.18 (0.09)	7.61 (0.07)	7.35 (1.85)	2.95 (0.28)
Na_2O*		3.60	3.04 (0.17)	3.32 (0.11)	1.73 (0.35)	1.65 (0.26)
K_2O		1.25 (0.29)	1.21 (0.04)	1.27 (0.04)	1.26 (0.37)	
P_2O_5		0.75 (0.05)	0.68 (0.05)	0.70 (0.06)	1.26 (0.37)	
F		0.19 (0.02)	0.13 (0.01)	0.13 (0.00)		
Cl		0.37 (0.09)	0.44 (0.00)	0.42 (0.00)		
I		0.15 (0.01)	0.21 (0.01)	0.18 (0.00)		
Total		84.83	89.02	92.26	70.95	74.74
Mg no.		56.0	47.7	48.2	62.3	39.8
Na_2O as analysed		2.74 (0.29)				

*Na_2O for quenched melt from run 1923 was estimated from the mass balance of run products and starting composition. *n* equals the number of analyses used to calculate averages. Figures in parentheses are 1 sigma standard deviations calculated for replicate analyses. All runs were conducted at 1050 °C, excepting run 1539 which was conducted at 1000 °C.

Table 3. Nernst mineral/melt partition coefficients for Mount Leura and Southern Highlands (run 1541) amphiboles.

Run	1923		1941		1925		1541	
GPa	2.0		1.5		1.0		2.0	
Li7	0.18	(0.03)	0.16	(0.02)	0.189	(0.004)	0.13	(0.01)
Be9	0.21	(0.002)	0.18	(0.03)	0.23	(0.02)	0.40	(0.08)
B10	0.05	(0.011)	<0.08		0.10	(0.01)	0.30	(0.04)
Mg25	2.54	(0.13)	2.67	(0.16)	2.95	(0.10)	2.17	(0.10)
Al27	0.97	(0.04)	0.83	(0.09)	0.88	(0.01)	1.03	(0.03)
P31	0.018	(0.001)	0.07	(0.01)	0.043	(0.005)	0.04	(0.01)
Ca43	1.47		1.44		1.37		1.48	
Sc45	2.25	(0.23)	1.81	(0.13)	2.39	(0.15)	1.79	(0.07)
Ti49	0.89	(0.02)	1.21	(0.15)	1.61	(0.06)	0.94	(0.03)
V51	4.1	(0.4)	3.23	(0.22)	4.0	(0.5)	0.26	(0.01)
Cr53	7.0	(1.4)	5.23	(0.52)	11.9	(1.7)	3.27	(0.18)
Co59	2.1	(0.3)	1.9	(0.2)	1.92	(0.20)	1.76	(0.07)
Ni60	15.0	(2.8)	15.98	(0.94)	8.6	(1.2)	4.5	(0.2)
Cu65	0.74	(0.73)	2.33	(0.33)	1.6	(0.3)	0.14	(0.01)
Zn66	0.16	(0.03)	0.48	(0.05)	0.28	(0.05)	0.54	(0.04)
Ga69	0.30	(0.03)	0.67	(0.06)	0.55	(0.09)	0.51	(0.03)
Ga71	0.31	(0.03)	0.68	(0.06)	0.58	(0.1)	0.59	(0.04)
Ge74	0.50	(0.06)	0.91	(0.03)	0.80	(0.14)	0.66	(0.04)
As75	<0.026		0.03	(0.01)	0.04	(0.04)	0.60	(0.07)
Rb85	0.13	(0.02)	0.15	(0.01)	0.10	(0.01)	0.31	(0.01)
Sr86	0.287	(0.005)	0.39	(0.05)	0.49	(0.02)	0.42	(0.02)
Sr88	0.294	(0.006)	0.39	(0.05)	0.50	(0.01)	0.51	(0.03)
Y89	0.87	(0.15)	0.73	(0.10)	0.91	(0.03)	0.64	(0.02)
Zr90	0.114	(0.003)	0.21	(0.04)	0.24	(0.02)	0.17	(0.01)
Nb93	0.081	(0.003)	0.19	(0.02)	0.30	(0.01)	0.10	(0.004)
Mo98	0.06	(0.01)	0.14	(0.02)	0.20	(0.03)	0.12	(0.02)
Ag107	0.36	(0.13)	0.30	(0.06)	0.30	(0.06)	0.32	(0.03)
Cd111	0.35	(0.07)	0.58	(0.03)	0.34	(0.10)	1.3	(0.7)
In115	n. a.		0.81	(0.09)	0.85	(0.19)	0.52	(0.08)
Sn118	0.033	(0.001)	0.035	(0.003)	0.028	(0.003)	0.80	(0.06)
Sb121	0.001	(0.000)	0.017	(0.003)	0.012	(0.008)	0.00	
Cs133	0.003	(0.001)	0.09	(0.01)	0.004	(0.001)	0.00	
Ba137	0.184	(0.008)	0.25	(0.03)	0.28	(0.02)	0.36	(0.02)
La139	0.058	(0.012)	0.09	(0.01)	0.099	(0.005)	0.17	(0.01)
Ce140	0.104	(0.002)	0.17	(0.02)	0.168	(0.004)	0.23	(0.01)
Nd146	0.25	(0.01)	0.36	(0.04)	0.41	(0.01)	0.43	(0.02)
Sm147	0.444	(0.005)	0.57	(0.06)	0.65	(0.03)	0.64	(0.02)
Tb159	0.74	(0.03)	0.76	(0.09)	0.89	(0.05)	0.78	(0.05)
Ho165	0.91	(0.14)	0.79	(0.10)	0.92	(0.08)	0.88	(0.03)
Tm169	0.99	(0.23)	0.71	(0.09)	0.84	(0.06)	0.58	(0.08)
Yb174	0.30	(0.02)	0.62	(0.10)	0.50	(0.07)	0.52	(0.06)
Lu175	1.00	(0.29)	0.63	(0.09)	0.72	(0.07)	0.61	(0.03)
Hf177	0.220	(0.001)	0.37	(0.07)	0.41	(0.05)	0.37	(0.04)
Ta181	0.087	(0.002)	0.20	(0.03)	0.30	(0.02)	0.12	(0.01)
W183	0.013	(0.003)	0.007	(0.001)	0.023	(0.001)	0.024	(0.004)
W184	0.009	(0.001)	0.012	(0.003)	0.006	(0.001)	0.024	(0.004)
Pb208	0.051	(0.004)	0.038	(0.004)	0.048	(0.010)	0.055	(0.010)
Bi209	0.002	(0.001)	0.29	(0.25)	0.08	(0.07)		
Th232	0.004	(0.000)	0.021	(0.005)	0.013	(0.001)	0.024	(0.004)
U238	0.005	(0.001)	0.021	(0.005)	0.014	(0.001)	0.031	(0.010)

Figures in parentheses are 1 sigma uncertainties propagated from the results of replicate analyses n.a. not analysed.

2.3. Analytical methods

The analytical methods used to analyse major, minor and trace elements in the Mount Leura starting glass and run products, and in amphiboles and melts from the haematite-magnetite buffered run 1541 on the Southern Highlands basanite are the same as those described by Adam & Green (2006). Major elements (Table 2) were analysed with a Cameca® SX50 electron microprobe. Trace and minor elements, and some major elements, were analysed with a laser microprobe coupled to an Agilent® 7500S ICP-MS. Amphiboles and glasses were ablated with a 30 μm diameter beam of UV light (λ = 266 nm). CaO was used as the internal standard for calibrating ICP-MS analyses. In each case, electron microprobe analyses of CaO were chosen from points close to the spots analysed by ICP-MS.

Table 4. Selected crystal and refinement data for synthetic pargasites.

Sample	SEQ	a(Å)	b(Å)	c(Å)	β(*)	V(Å^3)	R_{sym} %	R_{obs} %	R_{all} %	$\#F_{all}$	$\#F_{obs}$
1923	1099	9.868(1)	18.001(1)	5.296(1)	105.12(1)	908.1	1.7	2.0*	2.4	2055	1737
1941	1096	9.855(1)	18.013(1)	5.299(1)	105.05(1)	908.4	2.6	3.2*	4.3	2064	1649
1925	1097	9.843(1)	18.033(1)	5.302(1)	105.09(1)	908.6	1.7	2.2*	2.5	2059	1839
1541	1111	9.934(1)	18.026(1)	5.309(1)	105.43(1)	916.4	1.5	1.6	1.8	1384	1297
1539	1110	9.929(1)	18.029(1)	5.299(1)	105.33(1)	914.9	3.4	2.3	3.8	1388	1049
1447	1041	9.913(5)	18.049(6)	5.308(2)	105.36(3)	915.8	2.8	1.9*	2.2	2246	1208
1452	1114	9.932(1)	18.067(2)	5.309(1)	105.37(1)	918.5	2.2	2.2	2.6	2082	1827
1950	1112	9.879(1)	18.031(1)	5.296(1)	104.98(1)	911.3	3.7	3.4	5.4	2590	1843
1951	1113	9.898(1)	18.064(1)	5.303(1)	105.17(1)	915.2	3.9	3.4	5.3	2593	1959

Note: SEQ is the sequence number in the CNR-IGG-PV database; R are the standard disagreement indices calculated for the corrected intensities of equivalent monoclinic reflections (R_{sym}), and for the observed and calculated structure factors (F) of all the reflections (R_{all}) and of those used for the refinements ($I > 3\sigma_I$, R^*_{obs}; $I > 5\sigma_I$).

Minimum detection limits and 1σ errors for LAM ICP-MS analyses are similar to those reported by Adam & Green (2006). Mineral/melt partition coefficients calculated from the LAM ICP-MS data are given in Table 3. Propagated 1σ errors derived from replicate analyses of minerals and melts (Table 3) are up to several times larger than those attributable to counting statistics alone. Individual analyses of crystals and quenched melts have been deposited (Table A) and are available on request. Mineral/melt partition coefficients and analytical data for run products from the Bow Hill and Southern Highlands basanites are given in Adam & Green (1994, 2003, 2006).

2.4. X-ray data collection and structure refinement

Crystals were handpicked from the sections mounted in epoxy, and their crystal quality was checked first from optical and then from diffraction behaviour. Data collections were done with an area-detector Bruker/AXS SMART-Apex diffractometer, using graphite monochromatised Mo$K\alpha$ X-ray radiation. Four batches of 840 images each (0.2° ω-rotation) were collected at different ϕ positions (0°, 90°, 180°, 270°). The crystal-to-detector distance was 4 cm. Intensity data were integrated using the SAINT program (Bruker®) and corrected for absorption using the SADABS program (Bruker®). Diffraction data for amphibole from sample 1539 were collected with a point-detector Philips PW1100 4-circle diffractometer using graphite-monochromatised Mo$K\alpha$ X-radiation. Two equivalent monoclinic reflections (hkl and $h\bar{k}l$) were measured and corrected for Lorentz and polarisation factors and for absorption before merging. Reflection profiles were integrated following the method of Lehmann & Larsen (1974) as modified by Blessing *et al*. (1974). Intensities were corrected for Lorentz-polarisation and absorption following North *et al*. (1968). Unit-cell parameters were calculated from least-squares refinement of d-spacings calculated for 60 rows of the reciprocal lattice by measuring the reflections in the range $-30 < \theta < 30°$.

The reflections with $\theta \leqslant 35°$ (38° for samples 1950 and 1951) were used in the unweighted full-matrix least-squares structure refinement on F. The program used is a locally modified version of program ORFLS (Busing *et al*., 1962) which was designed to deal with complex solid solutions (E. Cannillo, *pers. comm.*). Selected crystal and refinement data are provided in Table 4. Geometrical parameters relevant to the present discussion are reported in Table 5. Atomic coordinates and displacement factors have been deposited (Table B). A recalculation of the amphibole analyses based on the results of structure refinements is given in Table 6. The differences between the refined group-site scattering values and those calculated from the unit formulae are also reported in Table 6.

3. Experimental results

3.1. Run products

The amphiboles produced in experiments appear black when viewed with a hand-lens, but brown under strong magnification and (non-polarized) lighting. In plane polarized light, they show blue-green to yellow and brown pleochroism. Individual amphibole crystals are either rounded or blocky in form and 200–300 μm in diameter. The identity of coexisting crystal phases varies depending on run conditions and starting composition (see Adam & Green, 1994, 2003, 2006). In the case of the Mount Leura Basalt they include clinopyroxene (in all experiments), orthopyroxene (at 1.5 and 2.0 GPa), olivine (at 1.0 GPa) and garnet (at 2.0 GPa). The haematite-magnetite buffered run on the Southern Highlands basanite produced clinopyroxene and titano-magnetite, in addition to amphibole. The quenched melts from experiments vary in composition. Those from the Mount Leura Olivine Basalt are equivalent to hydrous olivine tholeiites, whereas melts from the Bow Hill and Southern Highlands Basanites have either hydrous nepheline basanite or hydrous nepheline hawaiite compositions.

To check for analytical consistency, an iterative procedure was used to calculate mass balances between major element concentrations in run products and starting compositions. These were also used to calculate H_2O concentrations in melts (assuming constant bulk H_2O concentrations during individual experiments), and to correct for Na_2O

Table 5. A comparison between the mean bond-lengths determined from structure refinement, the aggregate cation radii calculated from site populations and Shannon (1976) data, and the results of lattice-strain calculations (r_0 + 1.38).

Run	1923	1941	1925	1541	1442	1539	1446	1447	1452	1950	1951
structure refinement											
⟨T1-O⟩	1.666	1.668	1.669	1.671		1.666		1.671	1.672	1.662	1.666
⟨T2-O⟩	1.636	1.636	1.636	1.642		1.638		1.642	1.641	1.636	1.638
⟨M1-O⟩	2.079	2.080	2.078	2.081		2.078		2.080	2.083	2.082	2.078
⟨M2-O⟩	2.053	2.055	2.060	2.054		2.072		2.062	2.069	2.062	2.072
⟨M3-O⟩	2.070	2.071	2.068	2.075		2.068		2.072	2.074	2.072	2.068
$^{[8]}$⟨M4-O⟩	2.488	2.487	2.487	2.497		2.501		2.494	2.498	2.494	2.501
$^{[6]}$⟨M4'-O⟩	2.411	2.408	2.412					2.416			
⟨A-O⟩	2.929	2.927	2.925	2.946		2.935		2.940	2.940	2.929	2.935
⟨Am-O⟩	2.880	2.878	2.871	2.914		2.888		2.900	2.897	2.890	2.888
⟨A2-O⟩	2.634	2.619	2.609	2.650		2.633		2.612	2.629	2.616	2.633
aggregate cation radii + 1.38											
T1	1.691	1.693	1.694	1.696	1.691	1.696	1.698	1.687	1.691		
T2	1.642	1.642	1.642	1.648	1.644	1.648	1.647	1.642	1.644		
M1	2.098	2.093	2.089	2.103	2.094	2.099	2.094	2.083	2.090	2.096	2.086
M2	2.043	2.050	2.046	2.036	2.044	2.051	2.044	2.056	2.065	2.064	2.073
M3	2.113	2.113	2.113	2.112	2.106	2.112	2.112	2.100	2.112	2.110	2.110
$^{[8]}$M4	2.463	2.461	2.466	2.477	2.478	2.477	2.476	2.479	2.478	2.464	2.480
$^{[12]}$A	2.833	2.819	2.811	2.868	2.856	2.852	2.846	2.836	2.823	2.830	2.828
$^{[10]}$A	2.686	2.665	2.652	2.739	2.721	2.714	2.705	2.691	2.671	2.682	2.679
lattice-strain calculations (r_0 + 1.38)											
$M2^{+3}$	2.06	2.05	2.07	2.06						2.07	2.08
$^{[8]}M4^{+2}$	2.46	2.45	2.46	2.44	2.47		2.47	2.47	2.47	2.46	2.45
$^{[12]}A^{+1}$	2.89	2.87	2.87	2.85	2.84		2.84	2.83	2.82	2.90	2.90

loss during electron microprobe analyses of quenched melts. Although minor and trace elements were not used to constrain the relative proportions of minerals and melts, the agreement between calculated bulk run products and starting compositions for most non-siderophile trace and minor elements was very good (usually within a few percent). But for some of the siderophile and chalcophile transition elements (including Fe, Ni, Sn, Cu, Ag, Sb and Pb) there were significant shortfalls in the calculated bulk compositions. Most of these shortfalls may be due to alloying between transition elements and precious-metal capsules. In the case of graphite-lined capsules, this could have occurred if the graphite capsules leaked during experiments and allowed some of the melt phase to come in contact with the Pt of the outer capsules. However, the problem is one that seems to be common in hydrous experiments conducted in graphite capsules, but not in otherwise similar dry experiments, and so the cause of the material losses is uncertain.

The melt H_2O concentrations calculated from mass balances (Table 6) are in most cases within 1.0 wt. % of the shortfalls in the combined totals of electron microprobe and LAM-ICP-MS analyses (*i.e.* 100 minus the combined wt. % of major, minor and trace oxides, fluorides, chlorides and iodides). Where SIMS analyses of H are available (see Hauri *et al*., 2006) there is a similarly close match in the estimated H_2O concentrations. But for runs 1923, 1541 and 1539 the differences between the melt H_2O concentrations obtained from mass balances, and the shortfalls in analytical totals, are significantly larger. For runs 1923 and 1539 these differences are 1.88 and 3.74 wt. % respectively. However, these differences are associated with high absolute melt H_2O concentrations (14.15 and 18.67 wt. % respectively) and so do not represent gross relative errors. But for run 1541 the difference is 16.25 wt. %. This can only be attributed to significant porosity within the coarsely quenched melt that has caused low analytical totals for the electron microprobe. The alternative explanation of 27.0 wt. % H_2O in the original melt is inconsistent with the expected effect of this much H_2O on the bulk composition's liquidus temperature (*i.e.* the bulk composition should have been rendered super-liquidus). In contrast

Table 6. Crystal-chemical formulae and H_2O concentrations in coexisting melts for the amphiboles of this work.

		Mount Leura			Southern Highlands						Bow Hill	
Run		1923	1941	1925	1541	1442	1539	1446	1447	1452	1950	1951
GPa		2.0	1.5	1.0	2.0	2.0	2.0	1.5	1.0	0.5	2.0	1.0
°C		1050	1050	1050	1050	1050	1000	1050	1050	1000	1050	1025
T sites	Si	6.240	6.155	6.142	6.137	6.246	6.291	6.258	6.093	6.052	6.471	6.292
	Al	1.760	1.845	1.858	1.863	1.754	1.709	1.742	1.907	1.948	1.529	1.708
	sum T	8.000	8.000	8.000	8.000	8.000	8.000	8.000	8.000	8.000	8.000	8.000
C sites	Ti	0.234	0.308	0.378	0.143	0.198	0.203	0.286	0.291	0.364	0.220	0.383
	Al	0.700	0.605	0.603	0.464	0.539	0.571	0.512	0.229	0.223	0.411	0.284
	Cr	0.006	0.008	0.010	0.002	0.027	0.019	0.036	0.012	0.057	0.021	0.045
	FeIII	0.006	0.064	0.156	0.593	0.224	0.062	0.279	0.716	0.578	0.155	0.158
	FeII	0.846	0.917	0.752	0.277	0.521	0.825	0.467	0.299	0.566	0.734	0.708
	Ni	0.004	0.004	0.005							0.008	0.005
	Mg	3.204	3.094	3.096	3.488	3.491	3.320	3.420	3.453	3.212	3.452	3.417
	sum M1-3	5.000	5.000	5.000	5.000	5.000	5.000	5.000	5.000	5.000	5.000	5.000
B sites	FeII	0.175	0.181	0.167	0.149	0.209	0.248	0.216	0.153	0.103	0.046	0.075
	Mn	0.012	0.014	0.015	0.011	0.011	0.013	0.011	0.014	0.015	0.011	0.011
	Mg	0.166	0.175	0.123	0.079	0.000	0.000	0.000	0.000	0.000	0.277	0.106
	Ca	1.616	1.629	1.694	1.737	1.753	1.725	1.771	1.829	1.881	1.573	1.806
	Na	0.031	0.001	0.001	0.023	0.027	0.014	0.023	0.004	0.001	0.093	0.002
	sum M4	2.000	2.000	2.000	2.000	2.000	2.000	2.000	2.000	2.000	2.000	2.000
A sites	Na	0.711	0.779	0.753	0.609	0.652	0.676	0.687	0.696	0.663	0.739	0.766
	K	0.241	0.192	0.147	0.391	0.348	0.324	0.303	0.264	0.237	0.241	0.234
	sum A	0.952	0.971	0.900	1.000	1.000	1.000	0.990	0.960	0.900	0.980	1.000
W sites	OH	1.559	1.465	1.291	1.542	1.565	1.665	1.319	1.411	1.426	1.498	1.465
	F	0.088	0.094	0.121		0.027		0.035		0.036	0.101	0.094
	Cl	0.012	0.018	0.015		0.000		0.001		0.001	0.017	0.018
	I	0.006	0.006	0.006								
	O^{2-}	0.335	0.417	0.567	0.458	0.408	0.335	0.645	0.589	0.537	0.384	0.543
	sum W	2.000	2.000	2.000	2.000	2.000	2.000	2.001	2.000	2.000	2.000	2.000
eC	EMP	75.10	77.58	77.30	73.93	73.41	75.25	74.25	77.49	80.56	75.23	76.72
eB	EMP	39.50	39.75	40.08	40.09	41.07	41.43	41.56	40.95	40.68	37.28	39.64
eA	EMP	12.40	12.22	11.08	14.13	13.78	13.59	13.31	12.67	11.80	12.71	12.87
eC	SCXRD	74.31	77.81	76.96	76.06		80.04		78.03	80.31	78.41	77.43
eB	SCXRD	39.08	39.91	39.91	40.14		42.16		41.82	42.13	38.75	39.93
eA	SCXRD	12.56	12.70	12.45	14.46		13.77		13.24	13.35	12.75	13.37
ΔC		0.79	−0.23	0.33	−2.13		−4.79		−0.54	0.25	−3.19	−0.71
ΔB		0.42	−0.16	0.17	−0.05		−0.73		−0.87	−1.45	−1.47	−0.29
ΔA		−0.16	−0.48	−1.37	−0.33		−0.18		−0.57	−1.55	−0.04	−0.50
Wt. % H_2O in co-existing melts		14.4	9.8	6.3	12.8	13.0	18.7	6.2	6.5	6.7	14.1	10.3

The OH contents in Mount Leura amphiboles, Bow Hill amphiboles, and samples 1541, 1539, 1452 and 1447 were calculated from the refined M1-M2 distances (see text). The OH contents in samples 1442 and 1446 were determined from SIMS analyses of H (Hauri *et al.*, 2006). H_2O concentrations in co-existing melts were calculated from mass balances and run product modes (see Sect. 3.1). The notation eC (eB, eA) refers to the number of electrons per formula unit (epfu) at the C sites calculated based on EMP analysis or refined by single-crystal structure refinement (SCREF). ΔC is the difference (in epfu) between the two independent estimates.

(and this applies to all of the experiments described in this study) the melt H_2O concentration obtained by mass balance is consistent with both the observed phase relationships and the H_2O concentration originally added to the starting composition (10.0 wt. %). Very considerable care was taken when preparing each experiment to ensure that the latter was accurate. We therefore consider that the melt H_2O concentrations calculated from mass balances are reliable, and that in most cases they are within ± 1.0 wt. % of actual values.

3.2. Amphibole compositions

The amphiboles produced in experiments on the Mount Leura Olivine basalt are dominantly pargasites with vari-

able amounts of kaersutite component (from 24 to 35 mole %) according to the classification scheme of Leake *et al.* (1997). They also contain minor fluoro, chloro, iodo and presumably also bromo components (Br was added to the starting composition but was not analysed). The amphiboles from individual experiments are typically quite homogeneous with respect both to their major and trace element concentrations, although the compositional variation is generally slightly larger than that attributable to analytical errors alone.

The main compositional changes observed with increasing pressure and melt H_2O concentration in the three Mount Leura amphiboles of this work (Table 6) are:

- a decrease in Ti concentration (from 0.38 to 0.23 apfu) coupled with a decrease in dehydrogenation (namely, of the oxo component, O^{2-}) at the O3 site (from 0.57 to 0.33);
- an increase in the Si content (from 6.14 to 6.24 apfu). This is coupled with an almost constant Al_2O_3 content and hence with an increase in $^{[6]}$Al and $^{[6]}$Al/$^{[4]}$Al;
- an increase in the K content (from 0.15 to 0.24 apfu).

Other variables that decrease with both increasing pressure and melt H_2O concentration are the partition coefficients of I, Sr, Ba, Ti, Zr, Hf, Nb, Ta, and LREE.

Amphiboles from the Bow Hill and Southern Highlands basanites are also pargasite-kaersutite solid solutions, but are generally more calcic than the Mount Leura amphiboles. The effects of pressure on their compositions are similar to those described for the Mount Leura amphiboles. But in the case of the Southern Highlands amphiboles, the degree of dehydrogenation is not a consistent linear function of pressure. This follows a similarly non-linear relationship between melt-H_2O concentrations and pressure.

4. Discussion

4.1. Crystal-chemical changes as a function of pressure

In the synthetic pargasites described in this study, there are compositional trends that can be interpreted in terms of a structural response to increasing pressure. Although Al remains relatively constant, $^{[6]}$Al/$^{[4]}$Al increases as pressure increases. The incorporation of $^{[6]}$Al makes the M2 and M3 octahedra smaller ($^{[6]}$Al = 0.535 Å, $^{[6]}$Mg = 0.72 Å, $^{[6]}Fe^{2+}$ = 0.78 Å), whereas the incorporation of $^{[4]}$Al makes the tetrahedral sites larger ($^{[4]}$Si = 0.26 Å, $^{[4]}$Al = 0.39 Å). These changes are consistent with the well known principle that higher pressure favours more compact structures. The distribution of $^{[4]}$Al between the T1 and the T2 tetrahedra (which is interpreted as high-T disorder) was evaluated based on refined bond-lengths and site populations according to Oberti *et al*. (1995a). The ratio ^{T2}Al/^{T1}Al is almost constant, as expected from the small T range of the synthesis.

Interestingly, the unit-cell volume decreases only slightly when pressure increases from 0.5 to 2.0 GPa. However, significant changes in all the unit-cell parameters are observed, which are coherent with the changes in site populations discussed above. There is a marked shortening of the b edge (which is sensitive to the aggregate size of the octahedra). The c edge (which is sensitive both to composition and to the conformation of the double-chain of tetrahedra) also tends to shorten with increasing pressure, and increasing $^{[4]}$Al and $^{[6]}$Al/$^{[4]}$Al ratio (note that these parameters are relatively elevated in amphibole from the high fO_2 run 1541). In contrast, the a edge either shortens only slightly or even lengthens (in Mount Leura amphiboles) with increasing pressure. This is consistent with the observed increase in the K content at the A site (as measured by EMP and confirmed by structure refinement). The observed increase in the ^{B}(Fe, Mg) content with increasing pressure significantly decreases the volume occupied by the B-cations but increases the $\sin\beta$ value. We can conclude that the combination of the changes in the various site populations allows the incorporation of higher K contents at higher pressures without increasing the unit-cell volume.

The amount of partial dehydrogenation was estimated from the refined M1–M2 distances, following a method recently calibrated at the CNR-IGG Pavia. More detail of this method is given in Oberti *et al.* (2007). In brief, a comparison of more than 100 amphiboles for which both structure refinements and SIMS analyses of H are available shows a linear relation between the amount of the oxo component (O^{2-}) and the M1–M2 distance; this feature decreases repulsive interactions between the high-charged cations at these sites (those at M1 being involved in the local charge balance after dehydrogenation). The M1–M2 distance depends on other compositional factors, such as the M4 site composition, and different regression equations have been developed to calculate the oxo component in calcic (pargasite/kaersutite) and sodic-calcic (richterite) amphiboles. The discrepancy between the measured and calculated O^{2-} values for the amphiboles used to set up the method is within 10 %; the estimates given for the Mt. Leura samples may be biased by their higher ^{M4}(Mg, Fe) contents, which in principle might allow for higher O^{2-}contents than in the reference sampling. Table 6 shows that for most of our refinements, the Ti:O^{2-} ratios calculated by this method are slightly higher than 1:2. If the estimates of dehydrogenation are correct, some Ti is not involved in the local balance of dehydrogenation, and thus occurs at the M2 site. In amphibole from the haematite-magnetite buffered run 1541, Ti:O^{2-} is $\ll$ 1:2, and thus the measured dehydrogenation requires the presence of Fe^{+3} at the M1 and M3 sites, a feature that is confirmed by structure refinement results (namely, the refined mean bond-lengths and site-scattering values).

The amount of Ti assigned to the M1 site based on the calculated oxo component can be validated by comparing refined group site scattering results with those calculated from the unit formulae (Table 6). If we assign to the M1 site only the amount of Ti required to compensate for the estimated dehydrogenation, together with a mixture of Mg and Fe^{2+} calculated to reproduce the refined site-scattering values, we obtain calculated bond lengths shorter than the refined ones. This feature is coherent with the structural

effects of dehydrogenation, but discards the possibility of assigning all Ti to the M1 site (which would increase this discrepancy further). The Ti content exceeding $^1/_2$ O^{2-} is thus incorporated into the M2 site. Also, a small degree of Al disorder between the M2 and M3 sites cannot be discarded on the basis of comparison of the observed and calculated mean bond lengths. This feature would be consistent both with the amphibole bulk chemistry and with the high-*T* conditions of crystallization (Oberti *et al*., 1995b).

The major peculiarity of the Mt. Leura synthetic pargasites is the exceptionally high concentrations of small cations (Mg, Mn and Fe^{2+}) at the B sites (Table 6). This is compatible with the high pressures and temperatures condition of synthesis, but also reflects the influence of the olivine basalt starting composition. Indeed, the B sites in the Mt. Leura amphiboles are richer in Mg and Fe^{2+} than in amphiboles from the Bow Hill and Southern Highlands basanites. This feature implies significant differences in the size of the B polyhedron and in the shape of the electron-density. In fact, the ionic radii of Mg and Fe^{+2} (0.72–0.89 Å and 0.78–0.92 Å respectively in [6]- or [8]-fold coordination) are far smaller than that of Ca^{+2} (1.12 Å in [8]-fold coordination), and Mg and Fe^{+2} tend to assume a [6+2]-fold coordination. In a long-range perspective, such as that of the structure refinements (which averages over the studied crystal), the presence of distinct local environments for the M4 cations is indicated by the presence of a complex shape of the electron density, which can be best modelled only with two distinct sites (M4 and M4') with a total occupancy of 1 in the refined structural model (*cf*. Table B, deposited). The presence of small cations at the M4 site in amphiboles is reflected also by smaller values of the β angle, which is a measure of the displacement of the amphibole I-beams piling along the *a* edge. Actually, the amphiboles of this work have β angles in the range 105.00–105.43°, among the lowest found in the IGG-CNR database for pargasite/kaersutite. This feature and the relaxation of the *a*-edge with increasing K content keep the unit-cell volume nearly constant (the unit-cell volume is calculated as $a \times b \times c \times \sin\beta$).

A further peculiarity of Mt. Leura amphiboles is the high atomic displacement parameters observed for the oxygen atoms bonded to the M4 cation and building up the basis of the T2 tetrahedron (namely, O4, O5, O6). This feature is consistent with the static disorder detected at the M4 site, and also reflects the changes in the local conformation of the double-chain of tetrahedra occurring as a function of the nature of the M4 cation. Also, the atomic displacement parameter of the O7 oxygen atom, which links two T1 tetrahedra, is very high, and has the major component lying in the direction of the *c* axis. This feature suggests that the local environment of the O7 oxygen atom is strongly affected by the M4 site population in these high-*P* and high-*T* amphiboles.

A final remark concerns the A-site occupancies. As the pressure of crystallization increases, Na tends to be replaced by K, and the overall A-site occupancy increases. The same trend is observed for K (and Rb) in the Southern Highlands Basanite, and was also observed by Dalpe & Baker (2000) in their study of partitioning between amphiboles and mafic silicate melts. K has been shown to be stable in very high-*P* amphiboles (Yang *et al*., 1999) and clinopyroxenes (Harlow, 1996; Bindi *et al*., 2002), where it enters the crystal-chemically analogous $M4^{amph}$ and $M2^{cpx}$ sites. In the present case, the structure refinement does not provide any evidence of the occurrence of K at the M4 site. However, as noted above, the crystal-chemical changes produced by increasing pressure allow increased incorporation of K into A sites without an increase in the unit-cell volume.

4.2. The lattice-strain model

Onuma *et al*. (1968) studied element partitioning between pyroxene phenocrysts and their host volcanic rock matrix. They noticed that partition coefficients, when plotted on a log scale against cation radius, form a series of parabolic trends. Each parabolic series can be related to a particular crystallographic site within the pyroxene structure. This type of relationship has been found to be characteristic of many other minerals, including amphibole (*e.g.* Bottazzi *et al*., 1999; Blundy & Wood, 2003; Dalpe & Baker, 2000). Onuma *et al*.'s (1968) observations were explained and systematised by Blundy & Wood (1994), who built upon the theoretical work of Brice (1975) to formulate what is generally known as the lattice-strain model. This is described by the relationship:

$$D_i = D_0 \exp\left\{\frac{-4EN_A\left(\frac{r_0}{2}(r_i - r_0)^2 + \frac{1}{3}(r_i - r_0)^3\right)}{RT}\right\}. \qquad (1)$$

The relationship gives Nernst partition coefficients (D_i) for isovalent cations in crystals and melts as a function of the relevant cation radii (r_i), the optimum radius of the structure site of incorporation (r_0), the partition coefficient (D_0) of the ideal or fictive cation having radius r_0, and the Young's Modulus (E) of the site. N_A, R and T stand for Avogadro's constant, the universal gas constant and temperature (in K) respectively.

Adam & Green (2003, 2006) used the lattice-strain model to calculate r_0, D_0 and E values for amphiboles from the Bow Hill and Southern Highlands basanites. We also used it to calculate r_0, D_0 and E values for amphiboles from the Mount Leura basalt and run 1541 on the Southern Highlands basanite (Table 7). Examples of fitted solutions and original partition coefficient data are plotted in Fig. 1a for amphibole from run 1925.

When applying the lattice-strain model to our data a number of simplifying assumptions and strategies were necessary. Ideally the lattice-strain model is applicable to crystals whose cations and anions are held together by ionic bonds. It does not account for other types of bonding, localization of electrical charge, the effects of lattice distortion or the influence of the melt phase. Also, the three independent M octahedra, which have different sizes and cation preferences, are treated altogether in the lattice-strain model. Thus use of the model implies acceptance of both a degree of approximation and of exceptions to a predicted pattern of behaviour. On Onuma diagrams (plots of

Table 7. D_0, r_0 and E values, maximum D_0, optimum valence and ΔG^{coulb} calculated for amphibole lattice sites.

RUN	1923			1941			1925			1541		
	M1-3	M4	A	M1-3	M4	A	M1-3	M4	A	M1-3	M4	A
D_0^{+6}	0.001			0.012			0.006					
r_0^{+6}	0.60			0.60			0.60					
E^{+6}	7000			7000			7000					
D_0^{+5}	0.08			0.20			0.29			0.12		
r_0^{+5}	0.627			0.628			0.628			0.62		
E^{+5}	5000			5000			5000			3200		
D_0^{+4}	1.34	0.005		1.8	0.023		2.4	0.015		1.5	0.04	
r_0^{+4}	0.637	1.020		0.638	1.025		0.64	1.022		0.645	1.015	
E^{+4}	1500	600		1500	600		1500	600		1600	800	
D_0^{+3}	5.1	0.66		4.7	0.83		5.0	0.92		5.5	0.85	
r_0^{+3}	0.68	1.02		0.67	1.02		0.69	1.022		0.68	1.04	
E^{+3}	700	310		600	310		660	300		800	330	
D_0^{+2}	3.4	1.6	0.35	3.0	1.7	0.49	3.0	1.6	0.57	5.0	1.8	0.7
r_0^{+2}	0.69	1.08	1.5	0.67	1.07	1.5	0.67	1.08	1.49	0.64	1.06	1.44
E^{+2}	250	180	100	300	180	120	300	210	100	400	180	220
D_0^{+1}			1.41			1.35			0.91		0.6	3.3
r_0^{+1}			1.51			1.49			1.49		1.14	1.47
E^{+1}			75			80			63		90	110
Maximum D_0	5.6	1.9		4.5	1.9		5.5	2.1		6.9	1.9	
optimum valence	2.7	2.26		2.77	2.23		2.87	2.31		2.57	2.04	
ΔG^{coulb} (kJ)	8.7	21.6		6.3	15.5		7.6	18.9		7.3	11.9	

E^{+n} values for valences greater than 3 (for M4 sites) and 4 (for M1-3 sites) are estimates used only for the purpose of constraining D_0^{+n} and r_0^{+n} values, and should not be considered as reliable. The r_0 values for +6 ions in M1-3 sites are only constrained by their predicted relationship with r_0 values for other valences and similarly should not be considered as reliable. The D_0 values for +6 ions in M1-3 sites are only minimum estimates based on D values for W.

D_i versus cation radius) the partition coefficients of most elements follow smooth parabolic trends, consistent with the predictions of the lattice-strain model (usually within ± 20 % of fitted values). But Ni^{+2} and Cr^{+3} plot well above neighbouring isovalent cations, whereas Ga^{+3}, Sn^{+4}, Cd^{+2} and Cu^{+2} show converse behaviour. Sn, Pb, Bi, Cd and Tl were simply inconsistent in their behaviour. In each of these cases we assumed that there were specific factors (*e.g.* crystal-field and/or disequilibrium effects), unaccounted for by the lattice-strain model, that affected the measured partition coefficients. Thus these listed elements were not used to fit the lattice-strain model.

Because Mo, W, Sb and V can all exist in a variety of valence states, deciding on their probable valence states during experiments was a problem. In most cases the partitioning of Mo and Sb follow the partitioning of Nb and Ta. As the latter are usually assumed to be pentavalent and have similar pentavalent radii to Mo and Sb, we assumed that Mo and Sb were also pentavalent. In scheelite and wolframite W is hexavalent. As this seemed to accord with the very low partition coefficients that we obtained for W in our experiments we also assumed that W was hexavalent. In experiments on the Bow Hill nepheline basanite that were also conducted in graphite-lined capsules (Adam & Green, 2006), partition coefficients for V in olivine are relatively small (0.15–0.23). Therefore most of the V in experiments seems likely to have been present as V^{+3} rather than V^{+2}. This option also gives the smoothest and most consistent results when V is plotted on Onuma diagrams.

The Young's Modulus E, and r_0 could in most cases be determined from fits to Eq. (1). But for +5 cations in M1–3 sites, these values cannot be unequivocally constrained using the data for individual amphiboles. Therefore a broader and model dependent approach was necessary. We adopted Tiepolo *et al.*'s (2000) proposal that the radius of Nb^{+5} is slightly larger than that of Ta^{+5}, and also assumed that (for each site) there is a systematic relationship between r_0 values for +5 ions and those of ions with other valences (see Blundy & Wood, 2003). In addition, we assumed that the behaviour of +5 ions in the octahedral sites of amphiboles will be consistent with that of the same ions in the crystal-chemically equivalent M1 sites of clinopyroxenes, where E and r_0^{+5} values have been better constrained (see Adam & Green, 2006). For +6 ions we only have the partition coefficient data for W^{+6} which we used to constrain minimum values of D_0^{+6}.

No attempt was made to take account of split-site behaviour. Instead, a different approach was taken and we treated the M1, M2 and M3 sites as a single site, and averaged the two distinct A2 and Am sites to the central (A2/m = A) position, yielding a model with one six-fold and one ten-fold site. In this way, a coherent set of D_0^{+n} values could be obtained and later used to model electrostatic effects. A final point concerns partition coefficients for heavy rare earth elements (HREE) in run 1923. Run 1923 produced garnet as well as amphibole and pyroxenes. The effect of garnet in some experiments is to deplete the melt in HREE after the crystallization of amphiboles and/or

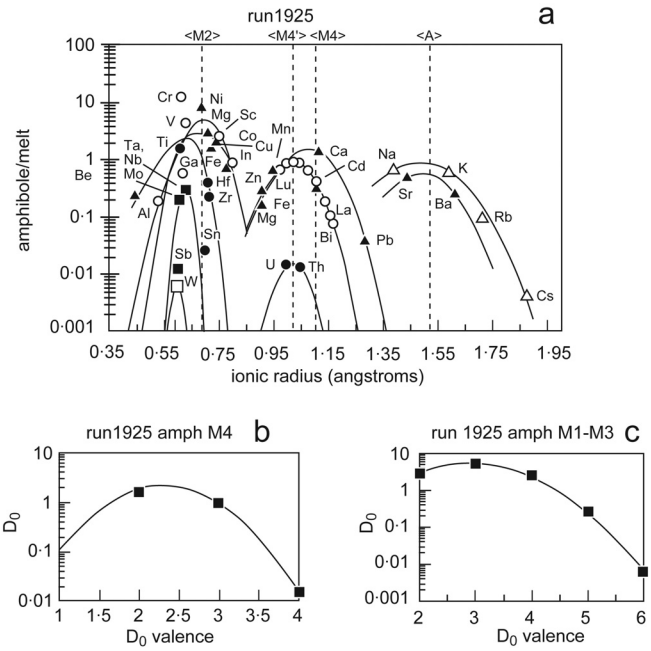

Fig. 1. Measured partition coefficients and fitted solutions to the lattice-strain model (dashed lines show site radii measured by X-ray diffraction) (a), and D_0^{+n} versus cation valence for the M1–3 and the M4 sites (b, c) in amphibole from run 1925.

pyroxenes, because D values for HREE in garnet are $\gg 1.0$ and garnet is usually the slower nucleating phase (for a description of a similar phenomenon involving zircon see Watson & Ryerson, 1986). When fitting Eq. (1) to the REE data for run 1923 we had to consider that the D_{HREE} were probably overestimated, and hence the calculated r_0^{+3}, D_0^{+3}, and E^{+3} values are less reliable.

4.3. A comparison of structure refinement results, aggregate cation radii, and lattice-strain calculations

Table 5 compares the mean the bond lengths of the T, M and A sites obtained by:

(a) structure refinement;
(b) the aggregate ionic radius calculated for major elements (⟨i. r.⟩) + 1.38 Å, *i.e.* the radius of O^{2-} in four-fold coordination (based on Shannon, 1976);
(c) lattice-strain calculations (r_0 + 1.38 Å).

The (a) and (b) sets represent values averaged over the studied crystals, but the first one takes into account relaxation effects due to local charge balance or steric hindrance consequent to solid solution. The third set represents the ideal dimension of the cation with a given valence state occupying each (aggregate) site. This comparison also allows a more detailed discussion of the crystal-chemistry and cation ordering in the pargasite-kaersutite solid solution.

The ⟨T-O⟩ distances estimated from Shannon's (1976) radii are always longer than the refined ones, especially for the T1 site (ΔT1 = 0.025, ΔT2 = 0.010 Å), confirming a significant covalent character of the T-O bonds. The calculated ⟨M1-O⟩ distances are smaller than the refined values, and account for structural relaxation due to dehydrogenation and partial repulsion between the high-charged cations occurring at the M1 and M2 sites. However, the good correlation between the two sets of values indicates that the assumed ordering of cations is correct. The largest differences between calculated and refined bond lengths are observed for the ⟨M3-O⟩ distances. This is expected because refined ⟨M3-O⟩ distances for Mg-rich pargasites are always smaller than would be predicted based on ionic radii; this feature allows for some Al disorder between M2 and M3 sites (Oberti *et al*., 1995b). The calculated r_0^{+3} values for the M1–3 sites are in good agreement with the refined ⟨M2-O⟩ distances, confirming that trivalent cations mainly occur at this site. The ⟨M4-O⟩ distances calculated using Shannon's radii are similar to the calculated r_0^{+2} values, but are smaller than the refined values. This is because Fe and Mg actually have a local [6] or [6+2] coordination (which is represented by the occurrence of the M4' site in the refined model). The agreement becomes good when this feature is taken into account.

4.4. The influence of valence on D_0^{+n}

When the D_0^{+n} values calculated for the M4 and M1–3 sites are plotted against valence, the resulting parabolic trends (Fig. 1a,b) are described by the equation

$$D_0^{n+} = D_0^{\Delta e=0} \exp\left(\frac{-\Delta G^{coulb} \Delta e^2}{RT}\right) \quad (2)$$

where: Δe is the cation valence ($+n$) minus the optimum site valence; ΔG^{coulb} is the coulombic potential energy produced by substituting a cation with a different valence; $D_0^{\Delta e=0}$ is the partition coefficient of the hypothetical cation having both optimum radius and optimum valence; $R$is the universal gas constant and T the temperature (in K).

This relationship was also used by Wood & Blundy (2001) to describe the effects of valence on trace element partitioning into the M2 sites of clinopyroxenes. The width of the parabola described by Eq. (2) is inversely related to ΔG^{coulb}. Hence, ΔG^{coulb} is always larger for the [8]- or [6+2]-coordinated M4 sites (15.5–21.6 kJ per mole) than for the [6]-fold coordinated M1–3 sites (6.3–8.7 kJ per mole). Similar differences in ΔG^{coulb} occur for the crystal-chemically analogous M1 and M2 sites in clinopyroxenes (Adam & Green, 2006).

4.5. Controls on the nature of the O3 anion

Variable H_2O contents were used in our experiments to maintain nearly constant degrees of crystallization, with increasing amounts of H_2O added to experiments with increasing pressure. Consequently, the effects of increasing pressure and increasing H_2O concentration overlap and can

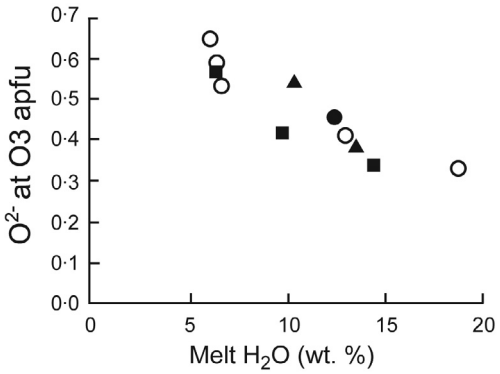

Fig. 2. Oxo component (O^{2-} at the O3 sites, apfu) versus melt H_2O concentrations for the amphiboles of this work. Solid black squares = Mount Leura, solid triangles = Bow Hill, open circles = Southern Highlands, solid circle = Southern Highlands with haematite-magnetite fO_2 buffer.

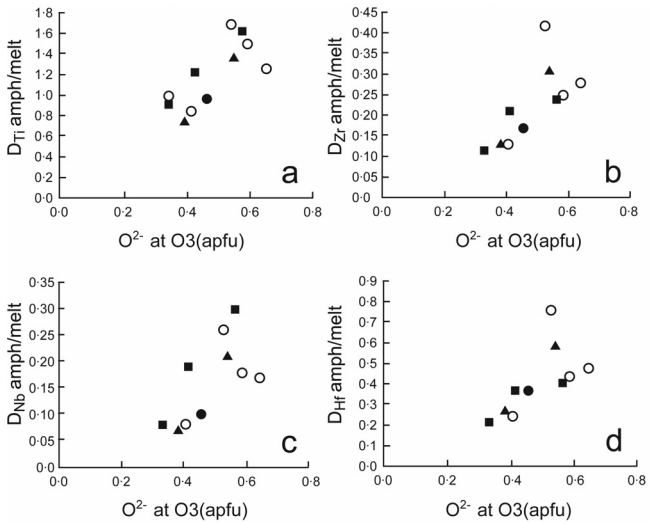

Fig. 3. Amphibole/melt partition coefficients for Ti (a), Zr (b), Nb (c) and Hf (d) versus O^{2-} at the O3 site (apfu). Symbols as for Fig. 2.

appear to be similar. This is shown by the degree of dehydrogenation at O3 which decreases as both pressure and melt-H_2O concentrations increase. However, if only experiments with near-constant melt H_2O concentrations are considered (*e.g.* runs 1446, 1447 and 1452), the effect of pressure turns out to be weak. In contrast, there is a strong negative correlation between melt H_2O concentration and O^{2-} at O3 (Fig. 2). It should be noted that in the case of the haematite/magnetite buffered run 1541 on the Southern Highlands Basanite (the solid circle), increased fO_2 does not result in a departure from the trend shown in Fig. 2.

Exchange K_Ds for the halides F, Cl and I (Table 8) indicate that they all partition into amphibole more strongly than H_2O. This will not, however, reflect the behaviour of OH^- ions, because most of the H_2O dissolved in the melts should be present as molecular H_2O (see Stolper, 1982; Silver *et al*., 1990). Thus exchange K_Ds for OH^- should be considerably higher than for H_2O. Whereas the overall halide concentration in amphibole seems to decrease as pressure increases, there are no clear trends to constrain the partitioning behaviour of F, Cl and I. For the Mount Leura and Bow Hill compositions, F partitions most strongly followed by I and then Cl. In the Southern Highlands composition both the Nernst and exchange K_Ds for F are smaller than for the Mount Leura and Bow Hill amphiboles. The relative magnitudes of F and Cl K_Ds are also reversed.

Exchange K_Ds for F do not show any evident dependence on pressure, but may be sensitive to concentration because F concentrations in the Mount Leura and Bow Hill starting compositions were much higher than in the undoped Southern Highlands composition. Both Nernst and exchange K_Ds for I decrease with increasing pressure. This is consistent with the large size of the I^- anion. In contrast, exchange K_Ds for Cl appear to increase with pressure, and are largest for the Southern Highlands compositions. The only reasonable correlations of these effects are with the K content and with the *a* unit-cell edge. The crystal-chemical relationship between Cl and K in amphiboles has previously been discussed by Oberti *et al*. (1993), who noted that the substitution of Cl into amphibole involved the ordering of K and Cl pairs into adjacent A and O3 sites together with lattice expansion along *a*. They attributed this arrangement to a chemical rather than to a structural affinity. Presumably, the relatively strong partitioning of I into amphibole (in spite of the size of this anion) reflects the same affinity but is more constrained by steric hindrance.

4.6. The influence of bulk composition on amphibole/melt partitioning of non-volatile elements

We have already noted that in many of our amphiboles the relative proportions of Ti and O^{2-} at O3 are close to 1:2, consistent with the substitution $^{M1}Ti^{4+} + 2^{O3}O^{2-} \leftrightarrow {}^{M1}R^{2+} + 2^{O3}OH^-$. This preferential mechanism to achieve local charge-balance was demonstrated in a previous study of Fe-free synthetic kaersutites and pargasites by Tiepolo *et al*. (1999), but is observed in many partially dehydrogenated amphiboles. Generally positive correlations between $D^{amph/melt}$ values for Ti, Zr, Hf, Nb and Ta, and O^{2-} at the O3 sites (Fig. 3a–d), confirm that all HFSE play some role in balancing dehydrogenation, as already suggested by Oberti et al. (2000). Conversely, it can be expected that D_{HFSE} will be affected by dehydrogenation (which is itself a strong function of melt H_2O concentration). However, in spite of the general correlation between D_{HFSE} and O^{2-}, the measured O^{2-}/HFSE ratios are variable. For example, O^{2-}/Ti varies from 3.24 to 1.25. Consequently, HFSE concentrations must be affected by other factors in addition to dehydrogenation. In the case of amphibole from the haematite/magnetite buffered run 1541, which has the highest O^{2-}/Ti ratio, titanomagnetite was a co-crystallizing phase and both the amphibole and quenched melt are comparatively depleted in TiO_2. Thus the availability of Ti must also affect how much Ti is incorporated into amphiboles, independently of O^{2-} concentrations.

Table 8. Exchange K_Ds and Nernst partition coefficients measured for volatile species occupying the O3 site.

Run	1923	1941	1925	1442	1446	1447	1452	1950	1951
				amphibole/melt exchange K_Ds					
H_2O/(H_2O+halogens)	0.9	0.89	0.86	0.97	0.96	1.0	0.95	0.89	0.85
F/(H_2O+halogens)	4.4	4.9	4.6	2.4	1.9	3.0	4.2	5.2	
Cl/(H_2O+halogens)	1.1	1.0	0.6		6.6		7.6	1.6	0.4
I/(H_2O+halogens)	4.3	6.8	7.9						
				Nernst partition coefficients					
F	7.63	10.38	9.0	17.0	15.1		19.9	1.0	1.4
Cl	0.51	0.45	0.62	17.4	28.0		29.6	0.20	0.06
I	0.33	0.88	1.2						

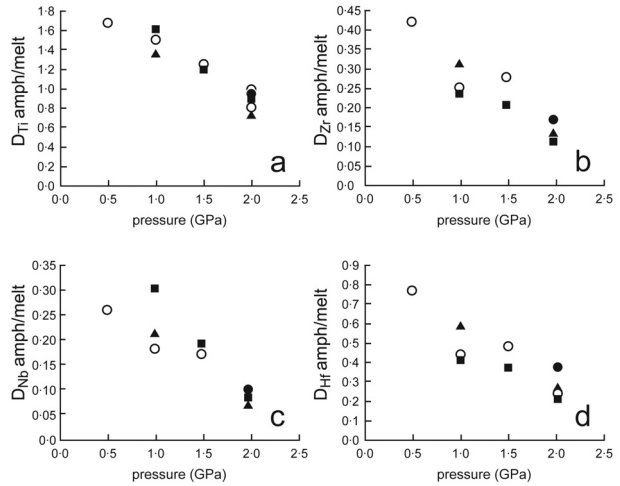

Fig. 4. Amphibole/melt partition coefficients for Ti (a), Zr (b), Nb (c) and Hf (d) versus pressure of synthesis (in GPa). Symbols as for Fig. 2.

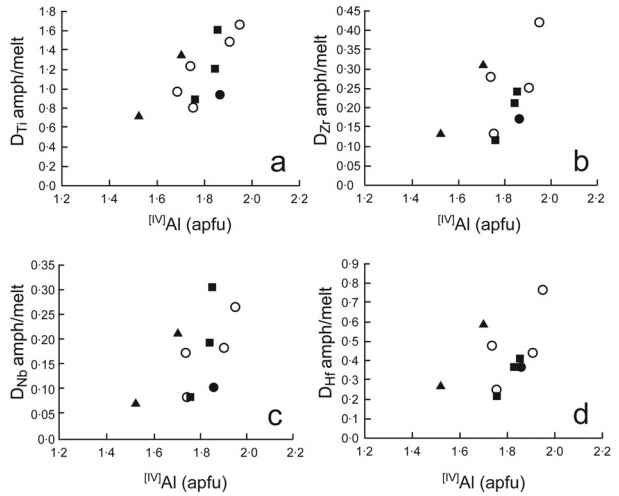

Fig. 5. Amphibole/melt partition coefficients for Ti (a), Zr (b), Nb (c) and Hf (d) versus [4]Al (apfu). Symbols as for Fig. 2.

One of the most consistent relationships observed both in this study and in others (*e.g.* Adam & Green, 1994, 2003; Dalpe & Baker, 2000; Fujinawa & Green, 1995) is the inverse correlation between D_{HFSE} for amphibole and pressure (Fig. 4a–d). This feature should be read as a direct correlation between D_{HFSE} and [4]Al (Fig. 5a–d), where the trends followed by amphiboles from the different starting compositions are variably displaced. Adam & Green (1994, 2003) and Fujinawa & Green (1995) explained the correlations they observed between D_{HFSE} and [4]Al by suggesting that the incorporation of high-charged cations at the M2 site allows local charge balance with the incorporation of [4]Al at T1. In the amphiboles of this work, at constant [4]Al, the highest D_{HFSE} values are found in amphiboles with the highest degree of dehydrogenation. On this basis, we confirm that D_{HFSE} increase both with [4]Al and with dehydrogenation, and thus that HFSE in pargasite-kaersutite solid-solutions are distributed between both M1 and M2 sites.

Partition coefficients for REE also correlate negatively with pressure and positively with [4]Al and [4]Al/[6]Al (Fig. 6a–d). Similar negative correlations between D_{REE} and pressure for amphibole and basaltic liquids were noted by Green & Pearson (1985) and Dalpe & Baker (2000). They also occur for U and Th (Table 3; see also Adam & Green, 2006). Adam & Green (1994, 2003) argued that the preferential incorporation of Al at the T1 site lowers the aggregate positive charge at both M2 and T1. Thus, the incorporation of high-charged cations at the M4 site is involved in local charge balance after the incorporation of [4]Al at adjacent T1 sites.

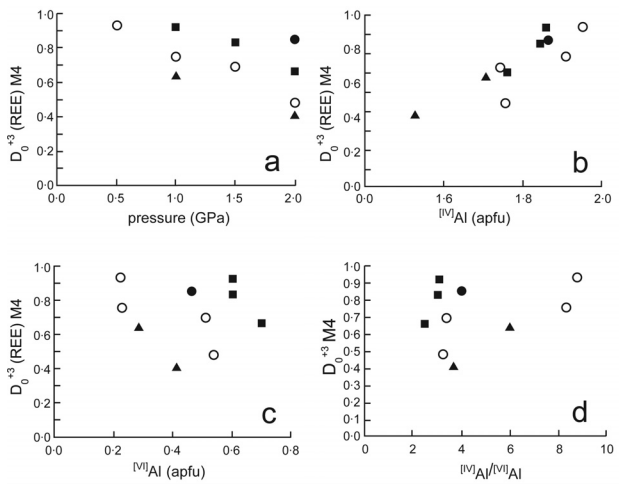

Fig. 6. D_0^{+3} for REE at the M4 site versus pressure (in GPa) (a), [4]Al (b), [6]Al (c), and [4]Al/[6]Al (d). Symbols as for Fig. 2.

4.7. Summary of conclusions

(a) With increasing pressure, amphiboles in equilibrium with hydrous basaltic and basanitic melts show a decrease in the *c* and (more strongly) *b* unit-cell edges. This feature reflects shortening of the ⟨T-O⟩ and ⟨M2-O⟩ mean bond distances, which in turn are due to a decrease in $^{[4]}$Al and an increase in $^{[6]}$Al. The *a* edge either decreases very little or actually increases as pressure increases. These variations in the unit-cell edges allow incorporation of K at the A site and Cl at the O3 site at near-constant unit cell volume.

(b) The OH^- content at the O3 site is a near linear function of H_2O concentrations in coexisting melts and is only weakly affected by variations in pressure and fO_2. F concentrations at O3 appear to be insensitive to pressure but are affected both by their absolute concentrations and by the ratio of F:H_2O in coexisting melts. Amphibole/melt partition coefficients for I decrease with increasing pressure at near constant I:H_2O in coexisting melts.

(c) r_0^{+3} values for the averaged M1–3 sites are close to measured ⟨M2-O⟩ distances consistent with the preferential incorporation of +3 cations at the M2 site. r_0^{+2} values for the M4 site are distinctly smaller than the refined ⟨M4-O⟩ distances. This latter feature can be explained as the result of averaging over two distinct M4 sites, one with [8] coordination, and the other (smaller) with [6] or [6+2] coordination.

(d) Amphibole/melt partition coefficients for the high field-strength elements Nb, Ta, Ti, Zr and Hf correlate positively with both $^{O3}O^{2-}$ and $^{[4]}$Al, consistent with the ordering of these elements at both the M1 and M2 sites according to two distinct coupled exchanges.

(e) Partition coefficients for REE, Th and U correlate positively with $^{[4]}$Al and $^{[4]}$Al/$^{[6]}$Al, but negatively with pressure. Because the calculated r_0^{+3} values of M4 sites are relatively constant, this is consistent with a dominantly electrostatic control over these pressure-related variations in the partitioning of REE, Th and U.

Acknowledgements: This research was supported by an ARC Small Grant and a Macquarie University Research Grant to Trevor Green. We thank Dr Norm Pearson, Suzie Elhou and Carol Conning for their assistance with electron microprobe and LAM-ICP-MS analyses. We are grateful to Rob Roy for manufacturing the graphite capsules and associated furnace components used in this study. We are also grateful to Claude Dalpe and Win van Westrenen for their constructive reviews of this manuscript. This is publication number 498 in the Australian Research Council National Key Centre for the Geochemical Evolution and Metallogeny of Continents (GEMOC). This study used instrumentation funded by ARC, LIEF and DEST Systematic Infrastructure Grants, Macquarie University and industry. Funding from CNR to IGG-Unità di Pavia through the project TA01.04.02 is also acknowledged.

References

Adam, J. & Green, T.H. (1994): The effects of pressure and temperature on the partitioning of Ti, Sr and REE between amphibole, clinopyroxene and basanitic melts. *Chem. Geol.*, **117,** 210-233.

—, — (2003): The influence of pressure, mineral composition and water on trace element partitioning between clinopyroxene, amphibole and basanitic melts. *Eur. J. Mineral.*, **15,** 831-841.

—, — (2006): Trace element partitioning between mica- and amphibole-bearing garnet lherzolite and hydrous basanitic melt: 1. Experimental results and the investigation of controls on partitioning behaviour. *Contrib. Mineral. Petrol.*, **152**, 1-17.

Adam, J., Green, T.H., Sie, S.H. (1993): Proton microprobe determined partitioning of Rb, Sr, Ba, Y, Zr, Nb and Ta between experimentally produced amphiboles and silicate melts with variable F content. *Chem. Geol.*, **109**, 29-49.

Bindi, L., Safonov, O.G., Litvin, Y.A, Perchuk, L.L., Menchetti, S. (2002): Ultrahigh potassium content in the clinopyroxene structure: An X-ray single-crystal study. *Eur. J. Mineral.*, **14**, 929-934.

Blessing, R.H, Coppens, P., Becker, P. (1974): Computer analysis of step scanned X-ray data. *J. Appl. Crystallogr.*, **7**, 488-492.

Blundy, J. & Wood, B.J. (1994): Prediction of crystal-melt partition coefficients from elastic moduli. *Nature*, **372**, 452-454.

—, — (2003): Partitioning of trace elements between crystals and melts. *Earth Planet. Sci. Lett.*, **210**, 383-397.

Bottazzi, P., Tiepolo, M., Vannucci, R., Zanetti, A., Brumm, R., Foley, S.F., Oberti, R. (1999): Distinct site preferences for heavy and light REE in amphibole and the prediction of $^{Amph/L}D_{REE}$. *Contrib. Mineral. Petrol.*, **137**, 36-45.

Boyd, F.R. & England, J.L. (1960): Apparatus for phase equilibrium measurements at pressures up to 50 kb and temperatures up to 1750 °C. *J. Geophys. Res.*, **65**, 741-748.

Brice, J.C. (1975): Some thermodynamic aspects of strained crystals. *J. Crystal Growth*, **28**, 249-253.

Busing, W.R., Martin, K.O., Levy, H.A. (1962): Report ORNL-TM-305. Oak Ridge National Lab., Tennessee. 75.

Dalpe C. & Baker, D.R. (2000): Experimental investigation of large-ion-lithophile-element-, high-field-strength-element- and rare-earth-element-partitioning between calcic amphibole and basaltic melt: the effects of pressure and oxygen fugacity. *Contrib. Mineral.Petrol.* **140**, 233-250.

Fujinawa, A. & Green, T.H. (1995): Partitioning of Hf and Zr between amphibole, clinopyroxene, garnet and silicate melts at high pressure. *Eur. J. Mineral.*, **9**, 379-391.

Green, T.H. & Pearson, N.J. (1985): Experimental determination of REE partition coefficients between amphibole and basaltic to andesitic liquids at high pressure. *Geochim. Cosmochim. Acta*, **49**, 1465-1468.

Green, T.H., Ringwood, A.E., Major, A. (1966): Friction effects and pressure calibration in a piston-cylinder apparatus at high pressure and temperature. *J. Geophys. Res.*, **71**, 3589-3594.

Harlow, G.E. (1996): Structure refinement of a natural K-rich diopside: The effect of K on the average structure. *Am. Mineral.*, **81**, 632-638.

Hauri, E., Gaetani, G.A., Green, T.H. (2006): Partitioning of H_2O between mantle minerals and silicate melts. *Earth Planet. Sci. Lett.*, **248**, 715-734.

Ionov, D.A., Griffin, W.L., O'Reilly, S.Y. (1997): Volatile-bearing minerals and lithophile trace elements in the upper mantle. *Chem. Geol.*, **141**, 153-184.

Irving, A.J. & Frey, F.A. (1984): Trace element abundances in megacrysts and their host basalts: constraints on megacryst genesis. *Geochim. Cosmochim. Acta*, **48**, 1201-1221.

Knutson, J., Sun, S.-S., Ewart, A. (1989): In: Johnson (Ed.) Intraplate Volcanism in Eastern Australia and New Zealand pp. 313-320, Cambridge University Press *in association with* The Australian Academy of Science, Melbourne.

Leake, B.E. (1997): Nomenclature of amphiboles: report of the subcommittee on amphiboles of the International Mineralogical Association Commission on New Minerals and Mineral Names. *Mineral. Mag.*, **61**, 295-321.

Lehman, M.S. & Larsen, F.K. (1974): A method for location of the peaks in step-scan-measured Bragg reflections. *Acta Crystallogr.*, **A30**, 580-586.

North, A.C.T., Phillips, D.C., Mathews, F.S. (1968): A semi-empirical method of absorption correction. *Acta Crystallogr.*, 12, 850-856.

Oberti, R., Ungaretti, L., Cannillo, E., Hawthorne, F.C. (1993): The mechanism of Cl incorporation in amphibole. *Am. Mineral.*, **78**, 746-752.

Oberti, R., Ungaretti, L., Cannillo, E., Hawthorne, F.C., Memmi, I. (1995a): Temperature-dependent Al order disorder in the tetrahedral double chain of C2/*m* amphiboles. *Eur. J. Mineral.*, **7**, 1049-1063.

Oberti, R., Hawthorne, F.C., Ungaretti, L., Cannillo, E. (1995b): $^{[6]}$Al disorder in amphiboles from mantle peridotite. *Can. Mineral.*, **33**, 867-878.

Oberti, R., Vannucci, R., Zanetti, A., Tiepolo, M., Brumm, R.C. (2000): A crystal-chemical re-evaluation of amphibole/melt and amphibole/clinopyroxene D_{Ti} values in petrogenetic studies. *Am. Mineral.*, **85**, 407-419.

Oberti, R., Hawthorne, F.C., Cannillo, E., Camara, F. (2007): Long range order. In: Amphiboles: Crystal Chemistry, Occurrence and Human Health edited by F. C. Hawthorne, R. Oberti, G. Della Ventura and A. Mottana. *Reviews in Mineralogy and Geochemistry*, **67**, 125-171.

Onuma, N., Higuchi, H., Wakita, H., Nagasawa, H. (1968): Trace element partitioning between two pyroxenes and the host lava. *Earth Planet. Sci. Lett.*, **5**, 47-51.

Rock N.M.S., Bowes D.R., Wright A.E. (1991): Lamprophyres, Blackie and Sons Ltd., New York, 285 p.

Shannon, R.D. (1976): Revised effective ionic radii in halides and chalcogenides. *Acta Crystallogr.*, **32A**, 751-767.

Silver, L. A., Ihinger, P.D., Stolper, E. (1990): The influence of bulk composition on the speciation of water in silicate glasses. *Contrib. Mineral. Petrol.*, **104**, 142-162.

Stolper, E. (1982): The speciation of water in silicate melts. *Geochim. Cosmochim. Acta*, **46**, 2609-2620.

Stolz, A. & Davies, G.R. (1988): Chemical and isotopic evidence from spinel lherzolite xenoliths for episodic metasomatism of the upper mantle beneath southeast Australia. *J. Petrol., Special Oceanic and Continental lithosphere Volume*, 303-330.

Tiepolo, M., Zanetti, A., Oberti, R. (1999): Detection, crystal-chemical mechanisms and petrological implications of $^{[6]}Ti^{4+}$ partitioning in pargasite and kaersutite. *Eur. J. Mineral.*, **11**, 345-354.

Tiepolo, M., Vannucci, R., Oberti, R., Foley, S., Bottazi, P., Zanetti, A. (2000): Nb and Ta incorporation and fractionation in titanian pargasite and kaesutite: crtstal-chemical constraints and implications for natural systems. *Earth Planet. Sci. Lett.*, **176**, 185-201.

Varne, R. (1970): Hornblende lherzolite and the upper mantle. *Contrib. Mineral. Petrol.*, 27, 45-51.

Watson, E.B. & Ryerson, F.J. (1986): Partitioning of zirconium between clinopyroxene and magmatic liquids of intermediate composition. *Geochim. Cosmochim. Acta*, **50**, 2523-2526.

Wilkinson, J.F.G. & Hensel, H.D. (1991): An analcime mugearite-megacryst association from north-eastern New South Wales: implications for high-pressure amphibole-dominated fractionation of alkaline magmas. *Contrib. Mineral. Petrol.*, **109**, 240-251.

Wood, B.J. & Blundy, J.D. (2001): The effects of cation charge on crystal-melt partitioning of trace elements. *Earth Planet. Sci. Lett.*, **188**, 59-71.

Yang, H., Konzett, J., Prewitt, C.T., Fei, Y. (1999): Single-crystal structure refinement of synthetic ^{M4}K- substituted potassic richterite, $K(KCa)Mg_5Si_8O_{22}(OH)_2$. *Am. Mineral.*, **84**, 681-684.

Received 17 January 2007
Modified version received 4 May 2007
Accepted 18 July 2007